 Cytometry 32:317–326 (1998)

Automated Segmentation of Muscle Fiber Images Using Active Contour Models

Aleš Klemenčič, Stanislav Kovačič, and Franjo Pernuš*
Faculty of Electrical Engineering, University of Ljubljana, Ljubljana, Slovenia

Received 2 December 1997; Accepted 31 March 1998

The cross-sectional area of different fiber types is an important anatomic feature in studying the structure and function of healthy and diseased human skeletal muscles. However, such studies are hampered by the thousands of fibers involved when manual segmentation has to be used. We have developed a semiautomatic segmentation method that uses computational geometry and recent computer vision techniques to significantly reduce the time required to accurately segment the fibers in a sample. The segmentation is achieved by simply pointing to the approximate centroid of each fiber. The set of centroids is then used to automatically construct the Voronoi polygons, which correspond to individual fibers. Each Voronoi polygon represents the initial shape of one active contour model, called a snake. In the energy minimization process, which is executed in several stages, different external forces and problem-specific knowledge are used to guide the snakes to converge to fiber boundaries. Our results indicate that this approach for segmenting muscle fiber images is fast, accurate, and reproducible compared with manual segmentation performed by experts. Cytometry 32:317–326, 1998.

Key terms: automated cytometry; muscle fiber; digital image analysis; segmentation; Voronoi diagram; active contour models

Skeletal muscles are characteristically composed of muscle fibers with different structural and functional properties of endomysium, a thin connective tissue surrounding each fiber, and perimysium, a thick connective tissue surrounding bundles of fibers or fascicles. On the basis of staining properties for alkaline myosin adenosinetriphosphatase (ATPase), fibers are classified as slow-twitch type 1 fibers, which stain light, or fast-twitch type 2 fibers, which stain dark (6). Measuring the cross-sectional area of different fiber types is one of the most common ways to analyze the structure and function of healthy and diseased human skeletal muscles (6,17,18,25,26). An obvious prerequisite for the study of pathological and physiological conditions influencing the size of different fiber types is to obtain the best possible estimate of the limits of normality in healthy individuals comparable in age, sex, and muscle. For that purpose, the areas of a huge number of fibers have to be determined. For instance, in establishing the normal cross-sectional area values for the vastus lateralis, vastus medialis, and trapezius muscles, approximately 18,000, 13,000, and 25,000 fibers, respectively, were measured (19,25,28). To determine the size of each fiber in a sample, the image of a muscle cross section, a complex pictorial scene, has to be segmented, that is, partitioned into its constituent parts—the muscle fibers.

Any segmentation procedure falls into one of the following categories: manual, semiautomatic, or fully automatic. There are several reasons why it is difficult to extract the desired fiber contours from the image automatically. In many cases, the muscle fibers are separated by connective tissue, which might be so thin that it cannot be detected or it might even be nonexistent. In such cases, if enough fibers of the same type are next to each other, they form clumps. Because of the lack of homogeneity in a specimen thickness, the microscope, and camera optics, the background brightness is heterogeneous. The gray values of pixels forming a fiber also can vary to a great extent. For these reasons, manual segmentation, facilitated by a graphic tablet or a computer mouse, was applied in most studies of muscle fibers (12,17,19,25,27). Manual methods are time-consuming, tedious, and suffer from a low degree of reproducibility (7). On the average, the manual segmentation of 200 fibers takes 20–30 min. The semiautomatic methods can be of two kinds: automated first guess, followed by manual editing or manual rough delineation, followed by automatic contour definition

Contract grant sponsor: The Rector's Foundation, University of Ljubljana.
*Correspondence to: Franjo Pernuš, Tržaška 25, 1000 Ljubljana, Slovenia.
E-mail: franjo.pernus@fe.uni-lj.si

(3,13,29,30). The first of these methods requires intensive manual post-processing, which may take the same amount of time as the manual method.

The present paper follows the latter approach. We have explored the idea of active contour models or snakes, introduced by Kass et al. (14), which have proved to be a promising (semi)automatic segmentation technique (4,5,8,20,21). Using snakes, accurate tracking of most fiber boundaries is achieved by simply pointing to approximate fiber centroids. The set of user-defined centroids is then applied to automatically construct the Voronoi polygons, which correspond to individual fibers. Each Voronoi polygon represents the initial shape of one snake. In the energy minimization process, which is executed in several stages, different external forces and problem-specific knowledge are used to gradually lead the snakes to the desired position. The proposed method requires limited user interaction, thereby saving a lot of time, and provides reproducible results.

MATERIALS AND METHODS

Muscle Sample Preparation

The vastus lateralis muscle of a previously healthy 23-year-old man was excised from the right leg 22 h after a sudden death. A slice, about 10 mm thick, was cut from the whole muscle on the border between the middle and distal third of the femur. Three blocks, each measuring approximately 1 cm^3, were cut from the superficial region and three from the deep region of the muscle slice and frozen in liquid nitrogen. Myofibrillar adenosinetriphosphatase (ATPase) activity was demonstrated in a 10-μm transverse section with the calcium method at pH 9.4 (23).

System Description

The digitization and subsequent analysis of muscle fiber cross sections was performed by using a microscope system, which is an assemblage of commercially available hardware together with our custom software. The system consists of a universal microspectrophotometer UMSP30 (Opton, Oberkochen, Germany) to which a black-and-white charge-coupled device (CCD) video camera AVC-D7CE (Sony, Tokyo, Japan) with 756 × 581 picture elements is attached. The video output is connected to a Meteor (Matrox, Quebec, Canada) frame grabber that provides real-time image transfer to a personal computer with a Pentium 166-MHz processor.

Active Contour Models

The active contour models (snakes) proposed by Kass et al. (14) have attracted much attention as a technique for image segmentation, matching, and tracking anatomic structures (21). An active contour model is a planar curve defined by a set of connected points that iteratively move from an initial position so as to minimize some formulation of an energy functional associated with the snake. Features of the image (e.g., gray level or gradient) contribute to the energy terms of the snake, as do intrinsic properties of the contour, such as continuity and curvature. In this way, the active contour model can react to the image and move continuously, ensuring boundary continuity and smoothness as it locates the desired boundary. The snakes, which can fill in for missing and noisy boundary information, overcome the problem of many contour extraction techniques, which use local edge information and which must find appropriate constraints for continuity when edges are broken.

The evolution of an active contour model from an initial estimate to its final state is driven by iterative minimization of the energy functional E_{snake}, which is a function of internal and external energies (14):

$$E(v)_{\text{snake}} = \int_0^1 \{E_{\text{int}}[v(s)] + E_{\text{ext}}[v(s)]\}\, ds, \qquad (1)$$

where the position of the snake is represented parametrically by $v(s) = [x(s), y(s)]$, along contour s ($0 \le s \le 1$). The internal energy term (E_{int}) controls the elastic properties of the snake and is expressed by

$$E_{\text{int}}[v(s)] = \frac{1}{2}\left(\alpha \left|\frac{\partial v(s)}{\partial s}\right|^2 + \beta \left|\frac{\partial^2 v(s)}{\partial s^2}\right|^2\right), \qquad (2)$$

where the parameter α controls the amount of stretching the snake is willing to undergo and β controls the amount of flexing it will allow (14).

The external energy (E_{ext}) comes from the image and/or higher level processes and is responsible for the deformation and movement of a snake toward application-specific image features. Using the variational method, minimizing the energy functional gives rise to a Euler–Lagrange equation, which, discretized and solved iteratively, gives

$$\mathbf{v}_k = (\mathbf{A} + \gamma\mathbf{I})^{-1}[\gamma\mathbf{v}_{k-1} - \boldsymbol{F}(\mathbf{v}_{k-1})], \qquad (3)$$

where $\mathbf{v}_k = \{v_{1,k}, v_{2,k}, \ldots, v_{N,k}\}$ are the positions of N control points at iteration k; $\mathbf{A}$ is a pentadiagonal matrix, depending on the elasticity parameters α and β; γ is the step size parameter; and $\boldsymbol{F}(\mathbf{v}_{k-1})$ are the external forces at control points of the discretized snake. Internal forces provide regularization through the inverse of the positive definite matrix $(\mathbf{A} + \gamma\mathbf{I})$. The iterations are terminated when the active contour stops changing between iterations.

The main problems associated with active contour models are initialization (i.e., the selection of the initial position of control points $\mathbf{v}_0$), clustering of control points due to external forces, and shrinking due to internal forces. Next, we give solutions to these problems.

In order to get an understanding of our solution to the shrinking of active contour models due to internal forces, we consider a situation in which external forces are completely absent [$\boldsymbol{F}(\mathbf{v}_{k-1}) = 0$]:

$$\mathbf{v}_k = (\mathbf{A} + \gamma\mathbf{I})^{-1}(\gamma\mathbf{v}_{k-1}). \qquad (4)$$

According to Equation 4, the model will shrink into a single point, which is not desirable. In such situations, we prefer that the contour model is not active (i.e., $\mathbf{v}_k = \mathbf{v}_{k-1}$). To prevent the snake from shrinking, we suggest adding a

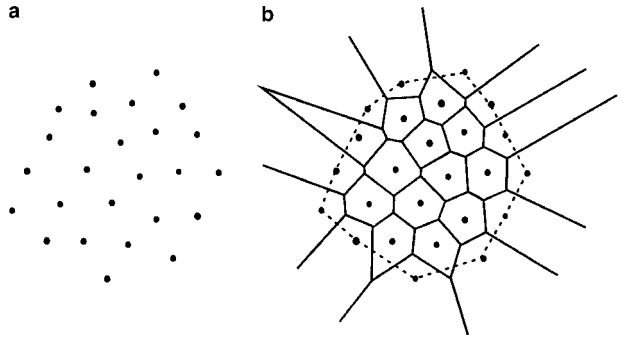

FIG. 1. **a:** A set of sites. **b:** The corresponding Voronoi diagram. The polygons corresponding to sites on the convex hull (dotted lines) are unbounded.

compensating force $\boldsymbol{F}_c(\mathbf{v}_{k-1})$ to Equation 4, giving

$$\mathbf{v}_k = (\mathbf{A} + \gamma\mathbf{I})^{-1}[\gamma\mathbf{v}_{k-1} - \boldsymbol{F}_c(\mathbf{v}_{k-1})]. \quad (5)$$

From Equation 5 and the condition $\mathbf{v}_k = \mathbf{v}_{k-1}$, we obtain the force $\boldsymbol{F}_c(\mathbf{v}_{k-1})$:

$$\boldsymbol{F}_c(\mathbf{v}_{k-1}) = -\mathbf{A}\mathbf{v}_{k-1}. \quad (6)$$

Adding the compensating force into Equation 3 and rearranging it gives

$$\mathbf{v}_k = \mathbf{v}_{k-1} - (\mathbf{A} + \gamma\mathbf{I})^{-1}\boldsymbol{F}(\mathbf{v}_{k-1}). \quad (7)$$

The above active contour model is implicitly stable, because only external forces may displace its control points (15).

In respect to the problem of clustering, we adopted the solution proposed by Lobregt and Viergever (20). Because the displacement of each control point $v_{i,k}$, ($i = 1, 2, ..., N$) along the path of the active contour model does not make any useful contribution to model deformation, the action of forces is constrained to the direction normal to the active contour. If we denote the locally normal component of the external force $\boldsymbol{F}(v_{i,k-1})$ as $\boldsymbol{F}_n(v_{i,k-1})$, then its length is given by the dot product of $\boldsymbol{F}(v_{i,k-1})$ and $\boldsymbol{n_i}$

$$\boldsymbol{F}_n(v_{i,k-1}) = [\boldsymbol{F}(v_{i,k-1}) \cdot \boldsymbol{n}_i]\boldsymbol{n}_i, \quad (8)$$

where $\boldsymbol{n}_i$ is the unit vector normal to the active contour model at point $v_{i,k-1}$. By replacing $\boldsymbol{F}(v_{i,k-1})$ in Equation 7 with $\boldsymbol{F}_n(v_{i,k-1})$, we obtain Equation 8, from which the muscle fiber boundaries are obtained.

$$\mathbf{v}_k = \mathbf{v}_{k-1} - (\mathbf{A} + \gamma\mathbf{I})^{-1}\boldsymbol{F}_n(\mathbf{v}_{k-1}). \quad (9)$$

The active contour model approach is an iterative energy minimization process that starts from an initial boundary defined by a set of control points, $\mathbf{v}_0 = \{v_{1,0}, v_{2,0}, ..., v_{N,0}\}$. If the initial boundary is placed too far from the solution boundary, the snake might converge erroneously to an undesirable shape. The initialization issue is application specific, requiring either prior knowledge or user interaction. Only few real-world images lend themselves to a fully automatic initial contour selection; therefore, some operator interaction, which should be reduced to minimum, is needed for most object segmentation purposes. We propose an automated initialization process for the muscle fiber images based on the Voronoi diagram.

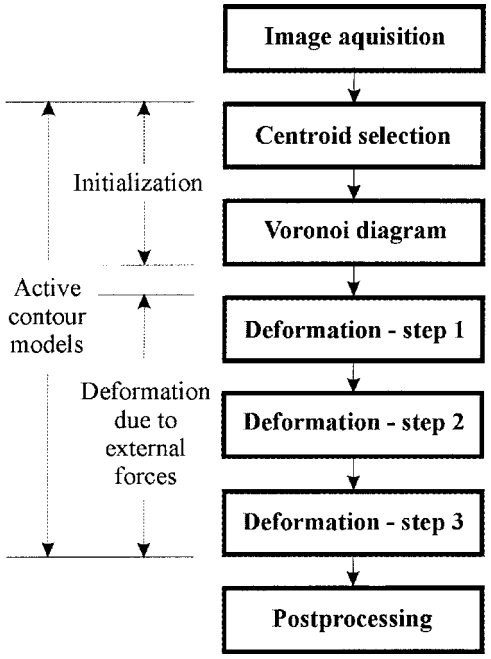

FIG. 2. Flow diagram of the proposed segmentation method.

Voronoi Diagram

One of the most basic geometric structures is the partition of space that is known in computational geometry as the Voronoi diagram (1). Let $P = \{p_1, p_2, ..., p_n\}$ denote a set of n distinct points, called sites, in the two-dimensional Euclidean plane. The plane is partitioned by assigning every point in the plane to its nearest site. Those points assigned to site p_i form the Voronoi region $V(p_i)$. Each region $V(p_i)$ ($i = 1, 2, ..., n$) therefore consists of all points in the plane at least as close to p_i as to any other site:

$$V(p_i) = \{x; d(x,p_i) \leq d(x,p_j), \forall j \neq i\}, \quad (10)$$

where d denotes Euclidean distance. Voronoi regions are convex and bounded polygons, except those that belong to the sites lying on the convex hull of P, which are unbounded. The Voronoi regions give a partition of the plane, called the Voronoi diagram for P and denoted as $V(P)$ (Fig. 1).

Segmentation Method

The proposed segmentation procedure is semiautomatic. Figure 2 summarizes the algorithm that has been used. Based on the set of manually defined centroids, the Voronoi polygons are derived and used as initial active contour models. Because of a complex scene, we use

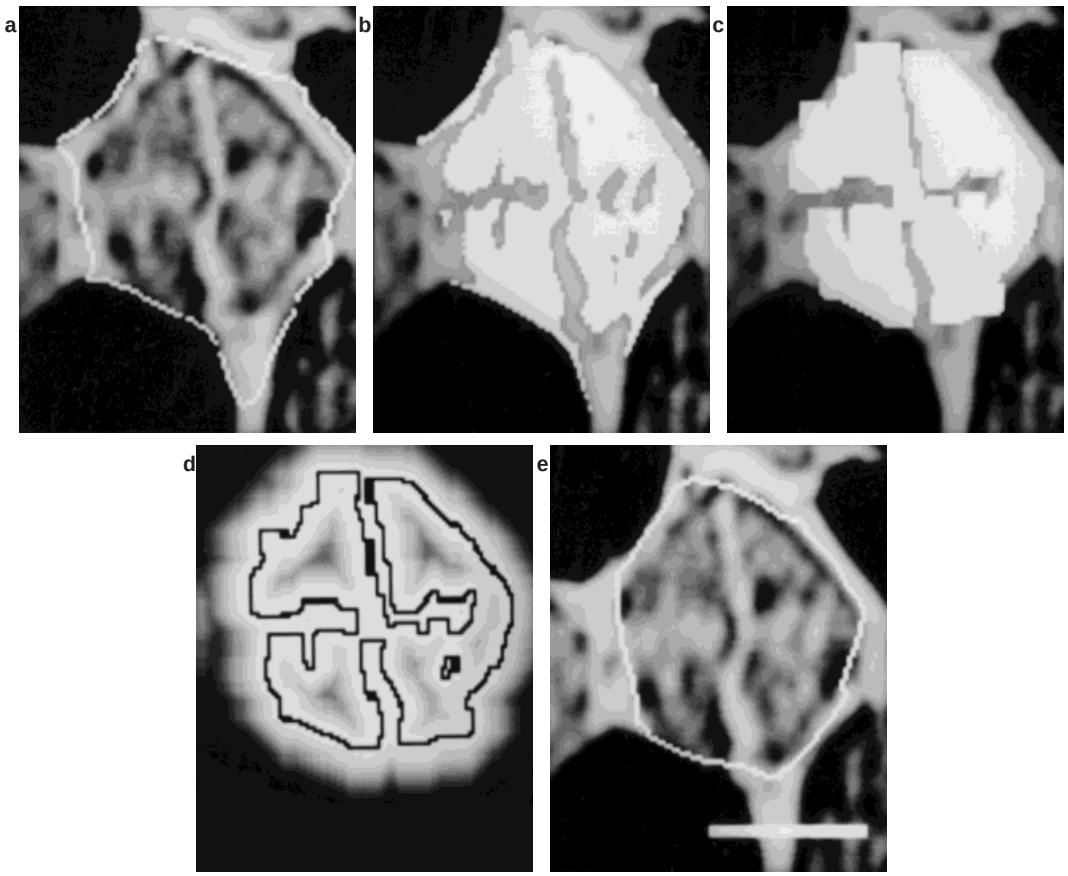

FIG. 3. **a:** A snake after deformation—step 1. **b:** The binarized area inside the snake. **c:** Filtered area of b. **d:** The edge of this area is used to calculate the distance map $D(x,y)$, which guides the deformation of the corresponding snake. **e:** The result of snake deformation—step 2. Scale bar = 50μm.

several different external forces and higher level knowledge to gradually lead the snakes to their final position.

Image acquisition. An artifact-free area of interest was selected from each muscle cross section, and the images were grabbed and stored as 512 × 360 pixel (1140 × 800 μm) images with 256 gray levels. This resolution (2.2 μm/pixel) enabled the correct segmentation of a scene, which was comprised of up to 200 fibers.

Initialization. In segmenting muscle fibers with snakes, we take advantage of the fact that the image we want to segment consists of tightly packed muscle fibers of approximately polygonal shape. The gaps between muscle fibers are mostly very thin and represent the endomysial connective tissue. Only in cases when the image consists of fibers from two or more muscle fascicles will these fibers be separated by a thicker connective tissue. The resemblance between muscle fibers and Voronoi polygons, first observed by Honda (11), led to the following snake initialization. An operator locates one point in the approximate center of each fiber. The set of points thus obtained represents the sites from which the Voronoi diagram is constructed. Only bounded polygons, which have all vertices inside the image, are kept. From each Voronoi polygon the initial control points of one snake are created automatically so that the control points are spaced 3 pixels (about 7 μm) apart.

Deformation step 1. Through experimentation, we have found that the parameter values $\alpha = 10$, $\beta = 20$, and $\gamma = 1$ yield an appropriate physical behavior of active contour models for our algorithm. These values were used in all three deformation steps. First, we let the initial active contours be attracted to intensity edges in a blurred muscle fiber image $I(x,y)$ by choosing the external forces $\boldsymbol{F}(\mathbf{v}_{k-1})$ as $\boldsymbol{F}(\mathbf{v}_{k-1}) = \nabla(-c_1 \mid \nabla[G_\sigma * I(x,y)] \mid)$, where ∇ is the gradient operator, $G_\sigma * I$ denotes the image convolved with a Gaussian smoothing filter whose characteristic width σ controls the smoothness, and the parameter c_1 controls the magnitude of the force $\boldsymbol{F}(\mathbf{v}_{k-1})$ such that it corresponds to about 1 pixel. The variance σ was successively reduced from 95 μm to 60 μm and 7 μm as iterations of the algorithm progressed (Equation 9). This procedure achieves a scale-space effect; that is, initially, the snakes are attracted to coarser edges from far away, and as the algorithm progresses, the attraction distance becomes smaller but the edge is better defined.

Deformation step 2. In muscle fiber images, the connective tissue is mostly brighter than type 1 and type 2 fibers, and this a priori knowledge was incorporated into

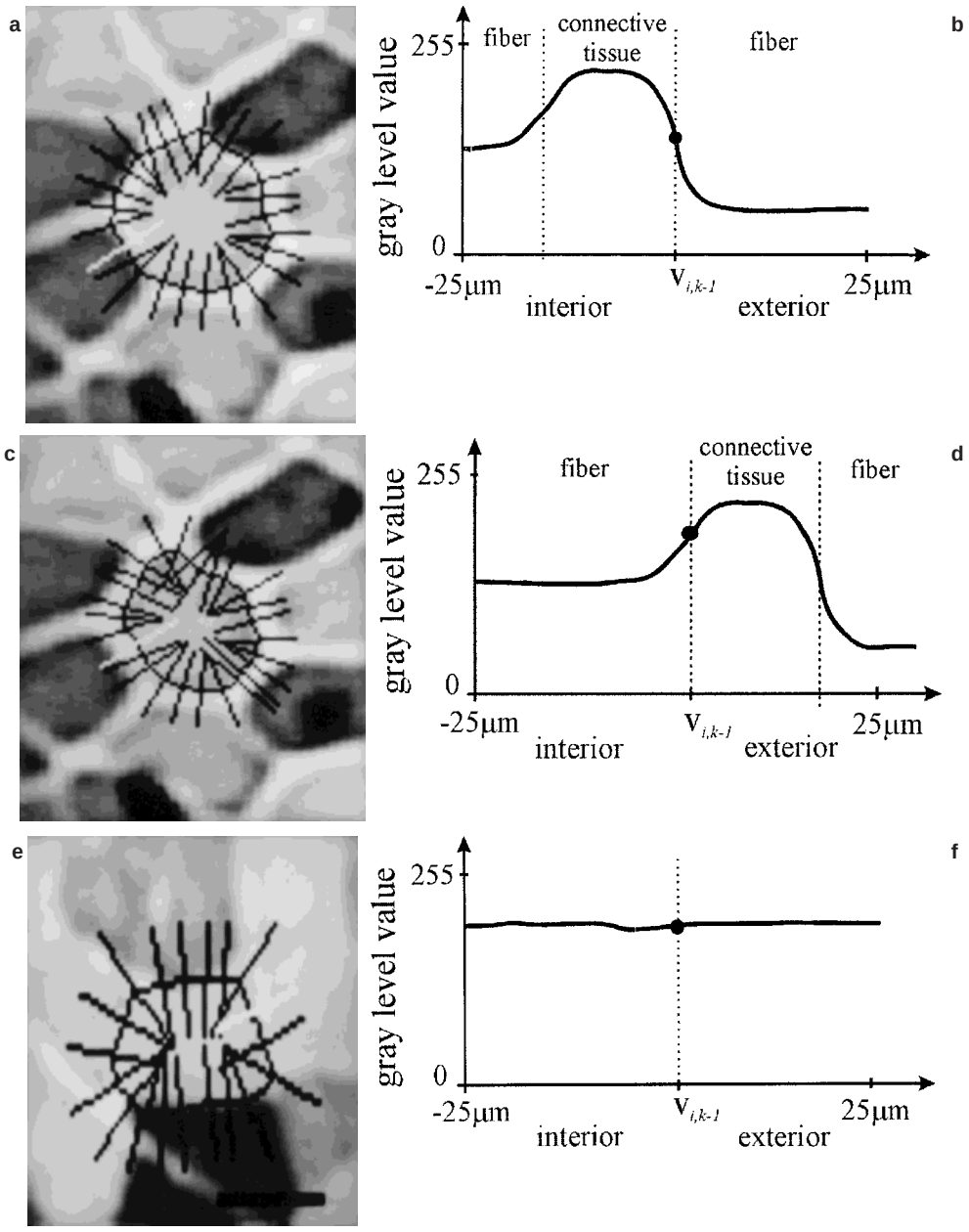

FIG. 4. **a**,**c**,**e:** Three snakes and the lines centered at control points normal to the curves. **b**,**d**,**f:** Gray-level value profiles along the white lines in a, b, and c, respectively. From the intensity profiles it can be inferred that the control point $v_{i,k-1}$ should be pulled inward (b) or it should not be moved (d and f). Scale bar = 50 μm.

the next stage of active contour models in the form of external forces, derived as follows. First, each muscle fiber region, defined by the snake from the previous stage, was binarized by applying a threshold to the gray values of pixels forming the region (Fig. 3a,b). For thresholding, we used the method proposed by Otsu (22), which automatically selects the proper threshold. Next, an opening (an operation of mathematical morphology) consisting of three iterations of erosion followed by three iterations of dilation was applied to each binary fiber region (10) (Fig. 3c). The opening is a filter that removes small details and smoothes the edge of a binary region. The edge of a binary region (Fig. 3d) was then used to define a distance-to-edge function $D(x,y)$ by assigning to each pixel the distance to the closest edge (2). The distance function with a continuous smooth gradient over the entire image guided the deformation of a corresponding snake (Fig. 3d,e), that is, $\boldsymbol{F}(\mathbf{v}_{k-1}) = -c_2 |\nabla D(x,y)|$, where c_2 again controls the magnitude of the force such that it is about 1 pixel. This step significantly improved the position of those snakes, which included large portions of connective tissue.

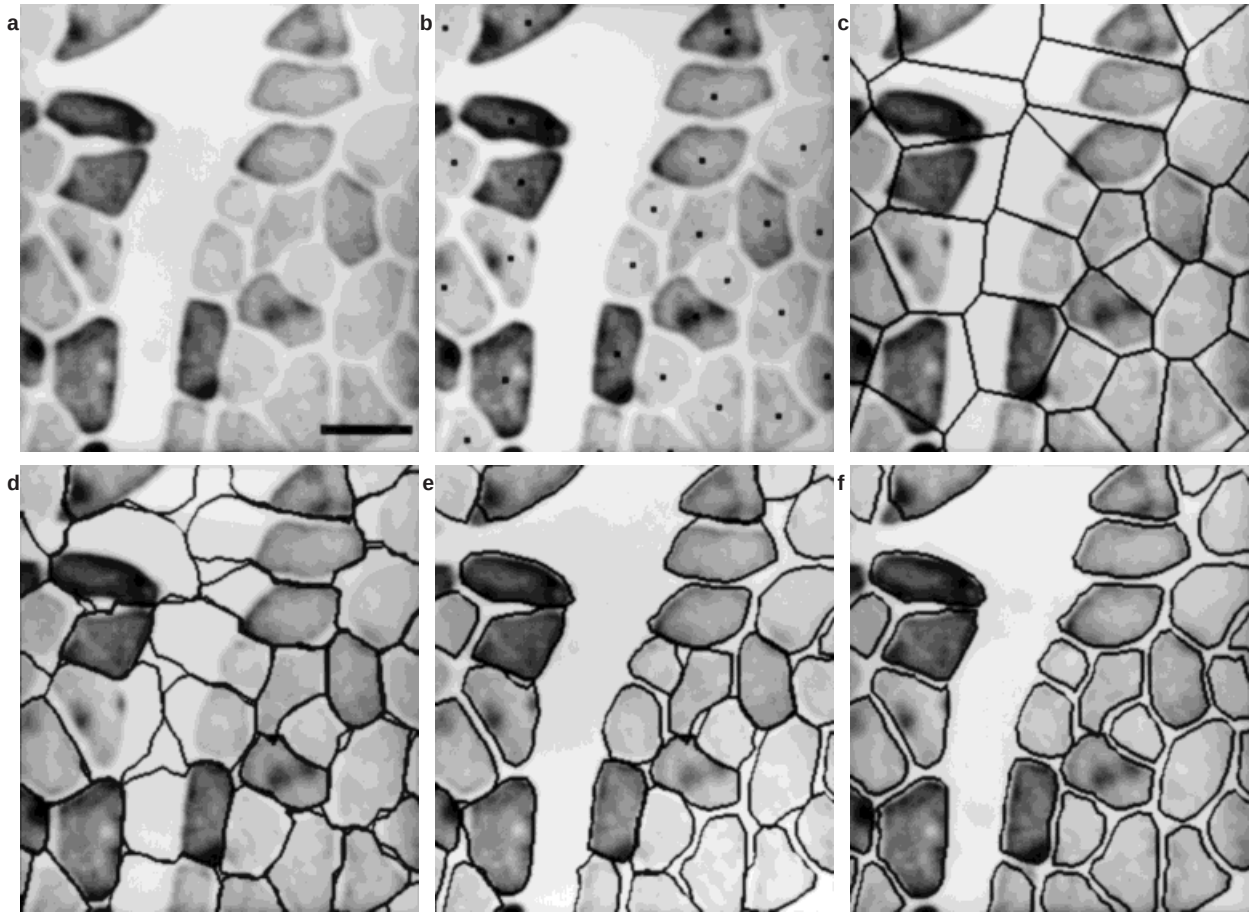

FIG. 5. **a:** A muscle fiber image. **b:** Manually selected centroids are superimposed on the image. **c:** The corresponding Vornonoi diagram. **d–f:** Results obtained after the 3 deformation steps. Scale bar = 100 μm.

Deformation step 3. In the final step, we again took advantage of the knowledge that connective tissue is mostly brighter than muscle tissue, but we did this even more locally than in the previous step. For each snake, which was the result of the preceding steps, we derived the gray-level value profiles along $(2w + 1)$ pixel-long lines. Each line was centered at a control point $v_{i,k-1}$ ($i = 1, 2, ..., N$) and directed outward from the interior of a fiber in the direction normal to the curve. Based on the analysis of the gray-level value profile, a control point $v_{i,k-1}$ was either moved in the direction of $\boldsymbol{n}_i$ [$\boldsymbol{F}_n(v_{i,k-1}) = c_3\boldsymbol{n}_i$] or $-\boldsymbol{n}_i$ [$\boldsymbol{F}_n(v_{i,k-1}) = -c_3\boldsymbol{n}_i$], or not moved [$\boldsymbol{F}_n(v_{i,k-1}) = 0$]. The parameter c_3 limits the force to about 1 pixel. Because the force $\boldsymbol{F}_n(v_{i,k-1})$ acts in the direction normal to the active contour, it is used directly in Equation 9. Because of the changing position of control points, profiles had to be recalculated before every iteration. Three characteristic profiles are shown in Figure 4. In the first case, the control point $v_{i,k-1}$ is attached to the edge of a neighboring fiber and has to be pulled inward. In the second case, the control point $v_{i,k-1}$ is at the edge of the corresponding fiber and therefore is not moved. The last case are two touching fibers of the same type. From the profile, it cannot be inferred whether the control point $v_{i,k-1}$ is inside one of the fibers or between them. Therefore, the control point is not moved.

Analysis of Algorithm Performance

Six muscle fiber images were shown, one by one, on a monitor. Two experts were asked to carefully delineate, using the mouse as the outlining device, each fiber in the images. The area of each fiber outline was defined as the number of pixels inside the outline. The a_i^1 values ($i = 1, 2, ..., M$, where M is the number of outlined fibers), areas obtained by the first expert, were taken as reference values, and a_i^2 ($i = 1, 2, ..., M$) represent the areas obtained by the second expert. Four users were then asked to mark the approximate centroids of the fibers outlined by the experts. For each user, a set of areas a_i^k ($i = 1, 2, ..., M$; $k = 3, 4, 5, 6$) was obtained from the final active contour models. No post-processing was done on the final results. For each fiber, the relative difference or error (e_i^k) between the reference area and the second expert's or one of the four users' area was defined as

$$e_i^k = \frac{a_i^k - a_i^1}{a_i^1} 100\% \qquad i = 1,2, \ldots ,M \qquad (11)$$

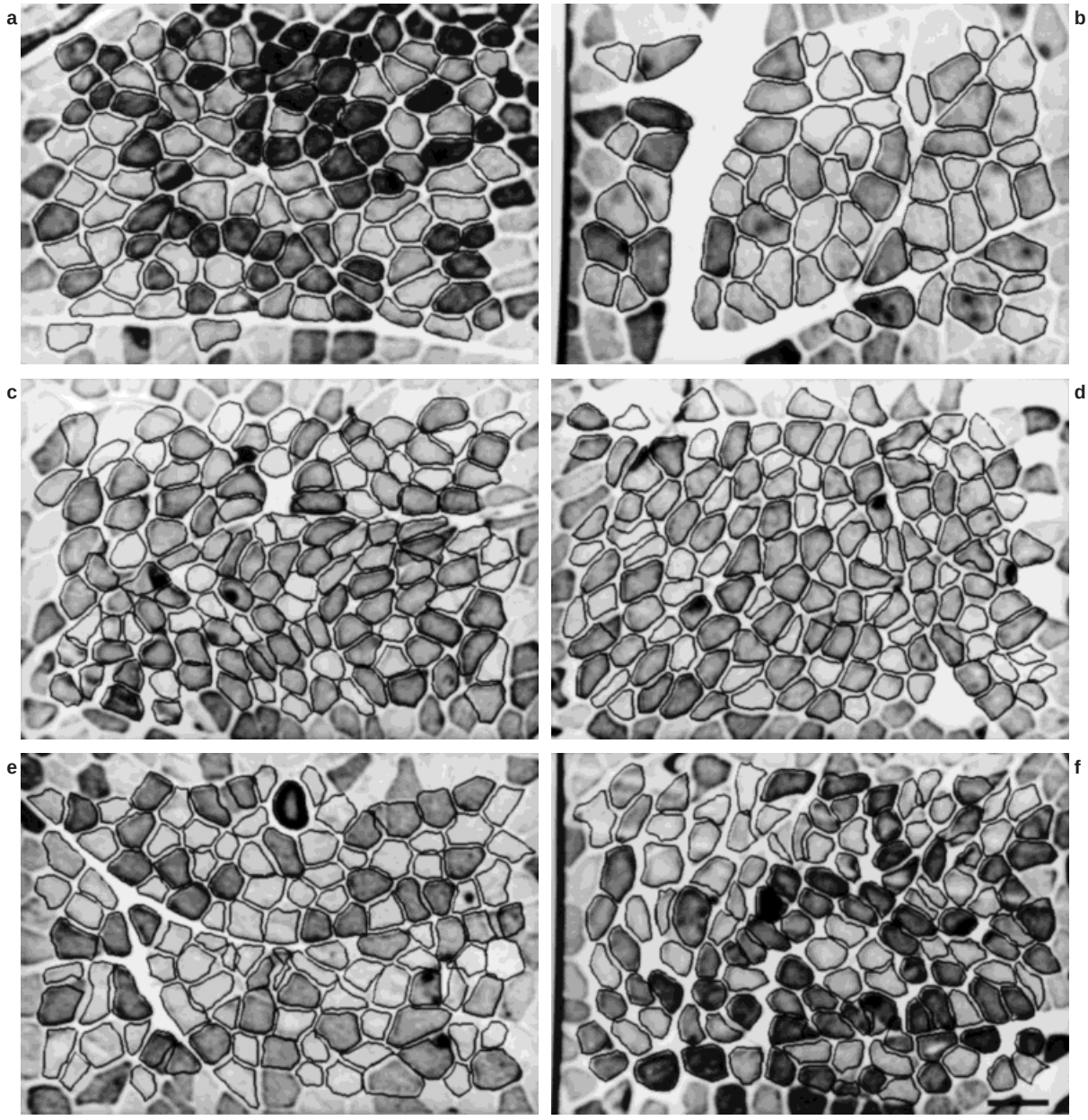

FIG. 6. **a–f:** The segmentation results of six muscle fiber images. Scale bar = 100 μm.

where $k = 2, ..., 6$ denotes the second expert and four users. The Kernel Density Estimator (KDE) method was used to obtain ''smoothed histograms,'' which allowed several distributions of errors to be displayed and compared easily on one graph (16).

RESULTS

Figure 5 illustrates the main steps of the described muscle fiber segmentation method. Figure 5a is a part of the image in Fig. 6b that contains the fibers to be segmented, and Fig. 5b shows the image with superimposed manually defined sites at the approximate centers of fibers. The sites were used to construct the Voronoi polygons, that is, the initial positions of active contour models (Fig. 5c). Because there is no free space between the Voronoi polygons, they inevitably include all the connective tissue. At places where the connective tissue is thick, the Voronoi edges are far from the fiber edges. A similarly poor initialization occurs at sites where a fiber's area and shape significantly differ from the area and shape of its neighbors. One can observe that at places where the connective tissue is thin and the fibers have similar shapes and sizes, the Voronoi polygons resemble the actual fiber contours quite well. Figure 5d shows the result of the deformation process of the active contour model after the first step of deformation. The snakes have reshaped, and

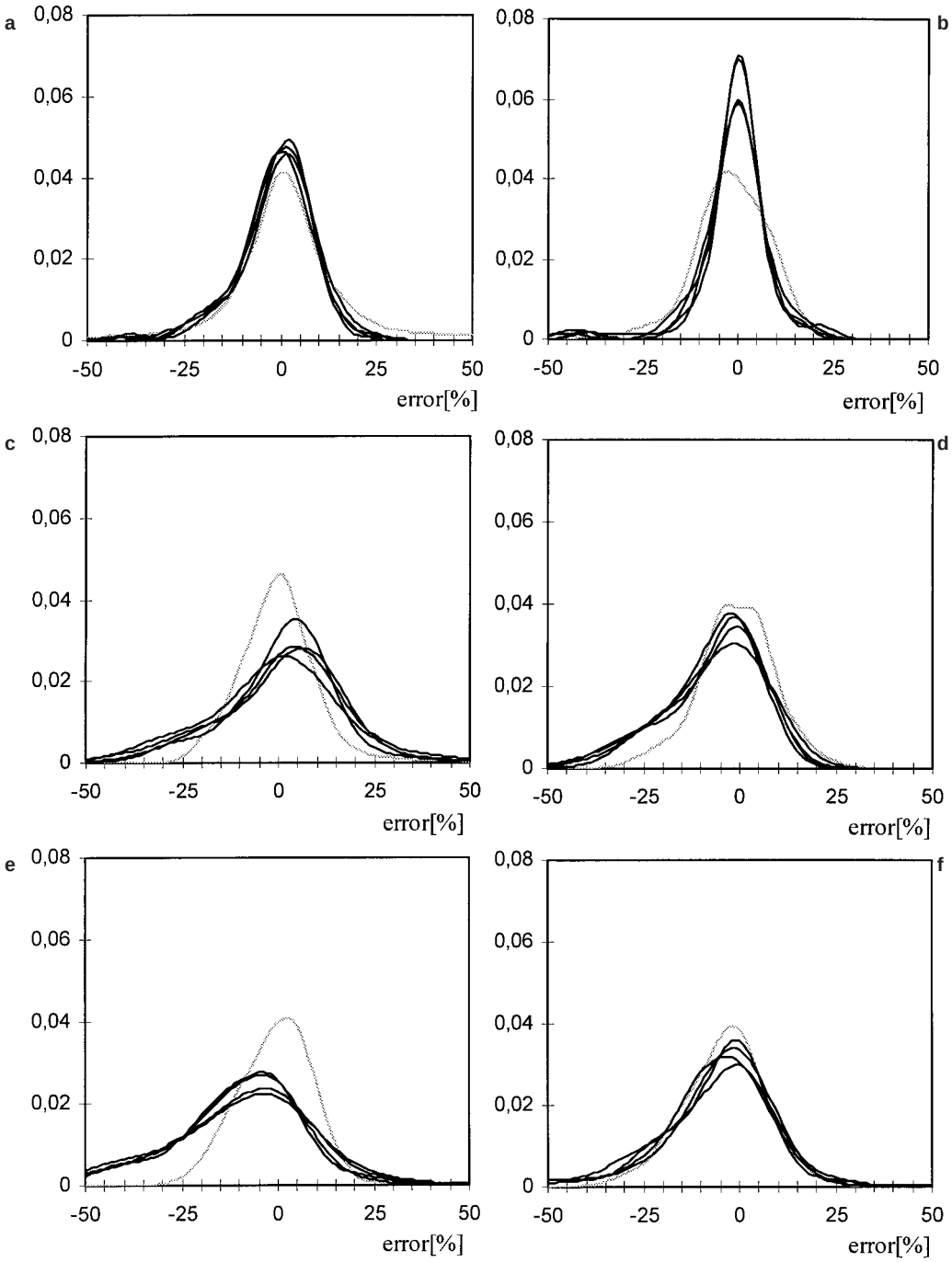

FIG. 7. **a–f:** The ''smoothed histograms'' of area differences between the first expert and the second expert (histogram in gray) and the first expert and the four users (histograms in black) for the six segmented muscle fiber images.

their shapes are much more natural; however, the snakes that were not close enough to fiber edges were not attracted to them but ended in undesirable local minima. Figure 5e shows the result after applying the external forces in the form of the gradient of a distance map. One can observe a great improvement, mainly in the sense that most of the connective tissue is excluded from the snakes. The results of the final step, in which the external forces were obtained by the cross-sectional analysis, are presented in Fig. 5f.

Figure 6 shows the results of applying the proposed algorithm to six muscle fiber images. As can be seen, the great majority of contours follow the muscle fiber boundaries very well. At some places, there are minor digressions

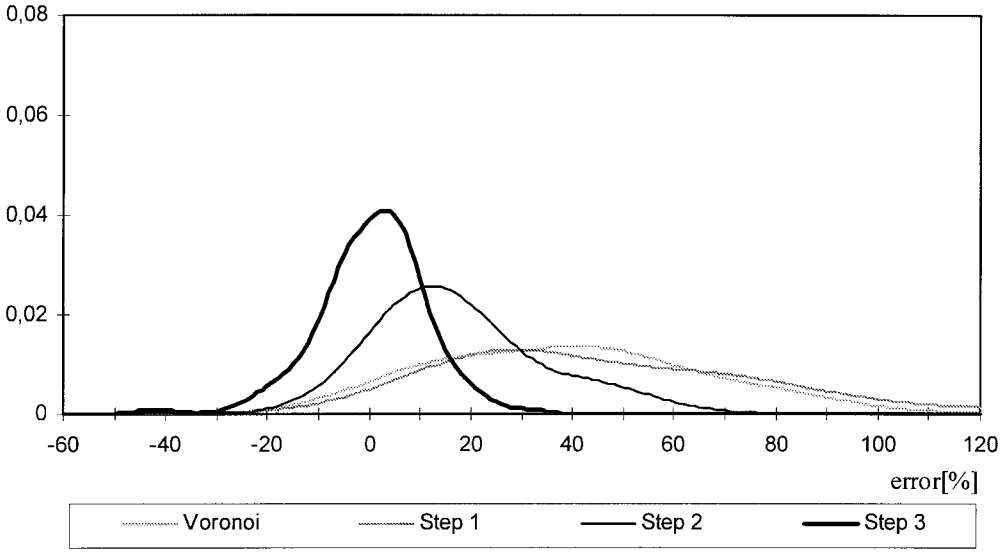

FIG. 8. The reduction of error during the segmentation procedure.

from the correct fiber edges, and only a few muscle fibers are falsely segmented.

The performance of the muscle fiber segmentation procedure was evaluated both qualitatively and quantitatively. An expert was asked to identify fibers in the segmented images that appeared to be falsely segmented, that is, for which the contours from the algorithm could not be accepted as they were without manual correction. The qualitative evaluation led to, on the average, 92% visually correctly segmented fibers. All fibers, including the ones judged by the expert as falsely segmented, were used in subsequent experiments.

We next show the sensitivity of the final segmentational results to the location of muscle fiber centroids—in other words, how reproducible the results are when starting from different sites. Figure 7 shows the distribution of errors for the six muscle fiber samples. The four histograms shown in black represent the errors e_i^k ($k = 3, ..., 6$) made by the proposed semiautomatic segmentation method starting from four different set of sites, each set entered by a different user. The gray histogram shows the distribution of errors made by the second expert (e_i^2). In each figure, the four histograms in black overlap very well, thus demonstrating that the location of sites, as long as they approximate the fiber centroids, has little influence on the final result. The differences between the solid lines and the gray line are very moderate, indicating that the automatic segmentation does not differ much from the segmentation performed manually by the second expert.

To get an impression of how much the individual segmentation steps improve the results, for one image (Fig. 6a) we show the ''smoothed histograms'' of errors (Fig. 8). The largest errors are obtained when the muscle fibers are approximated by Voronoi polygons. After each deformation, the error is reduced. The largest reduction is obtained after deformation steps 2 and 3 of the algorithm.

DISCUSSION

In this paper, we have presented a semiautomatic method for segmenting muscle fiber images. Our goal was to reduce the effort required to obtain the areas of a representative number of fibers from days to a few hours. We have approached this goal by using active contour models and Voronoi polygons to initialize them. The results presented here appear to be quite promising. This conclusion is supported by three facts: 1) the segmentation accuracy is comparable to that of manual tracing by trained observers, 2) minimal user interaction is required, and 3) the results are reproducible. In respect to the segmentation accuracy, we have to emphasize that the areas obtained by the semiautomatic method were not corrected manually and that when the results of any method are compared with reference data, inferior results always will be obtained if the reference is considered infallible.

Some work, however, remains to be done to improve the present prototype system. First, more fiber centroids have to be manually entered than there are fibers whose areas are determined because the Voronoi regions that are unbounded and that have a vertex outside the image are excluded from further analysis. This problem could be solved by either outlining the region of interest and using the outline to bound the unbounded Voronoi polygons or defining the shape hull of a set of sites (centroids) (24) and bounding the regions belonging to the sites on the shape hull. Second, in two steps of the algorithm we have assumed that the connective tissue is lighter than the muscle fibers. At locations where this assumption is violated, the fiber boundaries are erroneous. A double-staining technique (9) could help. It allows the visualization of myofibrillar ATPase activity on the same section under the microscope with transmitted light, and of the fluorescent staining that marks the outlines of the muscle

fibers by a simple switch to ultraviolet light. Third, our method requires minimal user interaction in the form of entering the fiber centroids. The question is whether muscle fiber segmentation can be done completely automatically. Most automated image segmentation procedures are based on certain assumptions about shapes, sizes, textures, and object and background intensities. These assumptions are often violated in muscle fiber images. However, in our future work, we will try to reduce the user interaction by automatically defining at least some fiber centroids. Finally, although we made no attempt to correct the falsely delineated fibers, the results are comparable to those obtained with manual boundary definition. The results could be improved by reinitializing the erroneous snakes by a rough manual delineation and by applying our algorithm, letting the snakes converge to their final positions.

The muscle fiber images used for this study, including the manually and semiautomatically defined boundaries, are available to other researchers in this field; please contact the corresponding author for more information.

LITERATURE CITED

1. Aurenhammer F: Voronoi diagrams: A survey of a fundamental geometric data structure. ACM Comput Surv 23:345–405, 1991.
2. Borgefors G: Distance transformations in digital images. Computer Vision, Graphics, and Image Processing 34:344–371, 1986.
3. Brenner JF, Zahniser DJ, Ziegelmiller DW, Adelman LS, Munsat TL, Bradley WG: Automated system for the analysis of muscle and nerve biopsies. Appl Optics 26:3398–3407, 1987.
4. Carlbom I, Terzopoulos D, Harris KM: Computer-assisted registration, segmentation, and 3D reconstruction from images of neuronal tissue sections. IEEE Trans Med Imaging 13:351–362, 1994.
5. Chalana V, Linker DT, Haynor DR, Kim Y: A multiple active contour model for cardiac boundary detection on echocardiographic sequences. IEEE Trans Med Imaging 15:290–298, 1996.
6. Dubowitz V: Muscle biopsy: A practical approach. Ballière Tindall, London, 1985.
7. Eilbert JL, Gallistel CR, McEachron DL: The variation in user drawn outlines on digital images: Effects on quantitative autoradiography. Comput Med Imaging Graph 14:331–339, 1990.
8. Fok Y-L, Chan JCK, Chin RT: Automated analysis of nerve-cell images using active contour models. IEEE Trans Med Imaging 15:353–368, 1996.
9. Hantai D, Albe X, Fardeau M: Double staining of the muscle fibers and interstitial tissue components for automatic analysis of muscle biopsies. Muscle Nerve 7:91–93, 1984.
10. Haralick RM, Sternberg SR, Zhuang X: Image analysis using mathematical morphology. IEEE Trans Pattern Anal Mach Intell 9:532–550, 1987.
11. Honda H: Description of cellular patterns by Dirichlet domains: The two-dimensional case. J Theor Biol 72:523–543, 1978.
12. Hopster DJ, Codd JD, Rose PE, Salisbury JR: Use of different histomorphometric parameters in the routine assessment of human skeletal muscle biopsies. Anal Cell Pathol 12:173–185, 1996.
13. Jain AK, Smith SP, Backer E: Segmentation of muscle cell pictures: A preliminary study. IEEE Trans Pattern Anal Mach Intell 2:232–242, 1980.
14. Kass M, Witkin A, Terzopoulus D: Snakes: Active contour models. Int J Comput Vision 1:321–331, 1988.
15. Klemenčič A, Kovačič S: Model Driven Snakes. Speech and Image Understanding. In: Proceedings of 3rd Slovenian-German and 2nd SDRV Workshop, pp. 311–320, 1996.
16. Lexell J, Taylor C: ''Smoothed histograms'': A visual aid for the analysis of distributions of muscle fiber areas. Muscle Nerve 14:826–828, 1991.
17. Lexell J, Taylor CC, Sjöström M: What is the cause of the aging atrophy? Total number, size and proportion of different fiber types studied in whole vastus lateralis muscle from 15- to 83-year-old men. J Neurol Sci 84: 275–294, 1988.
18. Lindboe CF, Platou CS: Disuse atrophy of human skeletal muscle: An enzyme histochemical study. Acta Neuropathol (Berl) 56:241–244, 1982.
19. Lindman R, Eriksson A, Thornell L-E: Fiber type composition of the human male trapezius muscle: Enzyme-histochemical characteristics. Am J Anat 189:236–244, 1990.
20. Lobregt S, Viergever MA: A discrete dynamic contour model. IEEE Trans Med Imaging 14:12–24, 1995.
21. McInerney T, Terzopoulos D: Deformable models in medical image analysis: A survey. Med Image Anal 1:91–108, 1996.
22. Otsu N: A threshold selection method from gray level histograms. IEEE Trans Syst Man Cyber 9:62–66, 1979.
23. Padykula HA, Herman E: The specificity of the histochemical method for adenosinetriphosphatase. J Histochem Cytochem 3:170–183, 1955.
24. Pernuš F: The Delaunay triangulation and the shape hull as tools in muscle fibre analysis. Pattern Recognit Lett 8:197–202, 1988.
25. Pernuš F, Eržen I: Fibre size, atrophy, and hypertrophy factors in vastus lateralis muscle from 18- to 29-year-old men. J Neurol Sci 121:194–202, 1994.
26. Schantz P, Randall-Fox E, Hutchison W, Tydén A, Åstrand P-O: Muscle fibre type distribution, muscle cross-sectional area and maximal voluntary strength in humans. Acta Physiol Scand 117: 219–226, 1983.
27. Scott KWM, Hoy J: The cross-sectional area of diaphragmatic muscle fibres in emphysema, measured by an automated image analysis system. J Pathol 120:121–128, 1976.
28. Travnik L, Pernuš F, Eržen I: Histochemical and morphometric characteristics of the normal human vastus medialis longus and vastus medialis obliquus muscles. J Anat 187:403–411,1995.
29. Wakisaka H, Hijikata T, Yohro T: Muscle fiber-type analysis aided by a personal computer. Biomed Res Tokyo 14:353–361, 1993.
30. Zukowski F, Collumbien R, Coen H, Roels F: Automated cytometry of muscle fibre sections: Size and spatial distribution of the four fibre types in young and adult rats. Anal Cell Pathol 3:273–286, 1991.